**Proceedings of ASME Turbo Expo 2019: Turbomachinery Technical Conference and Exposition**
**GT2019**
**June 17-21, 2019, Phoenix, Arizona, USA**

# GT2019-91654

# EVALUATING THE EFFECTS OF TRANSIENT PURGE FLOW ON STATOR-ROTOR SEAL PERFORMANCE

**Reid A. Berdanier, Eric T. DeShong, and Karen A. Thole**
Department of Mechanical Engineering
The Pennsylvania State University
University Park, PA 16802, USA

## ABSTRACT

As modern engine designs target higher efficiencies through increased turbine inlet temperatures, critical turbine components are at increased risk of damage from conditions exceeding material melting temperatures. In particular, improperly designed underplatform hardware components are susceptible to damage when hot main gas path flow is ingested into the stator-rotor cavity. While all turbines inherently experience transients during operation, a majority of turbine tests have been executed using steady operating conditions, and routine transient events are not well understood. To address this need, the present study utilizes a continuous-duration, one-stage test turbine operating with true-scale engine hardware and seal geometries at engine-representative flow conditions. The nature of the continuous-duration facility uniquely supports direct assessment of transient events through its ability to transition between steady-state operating conditions. Specifically, the effects of a transient purge flow were investigated in this study to identify general trends for transient events in a full-scale engine. Results from multiple measurement techniques in the wheelspace region show an interdependence of transient purge flow with a thermal lag of the underplatform hardware. Through experiments conducted at different coolant-to-main gas path temperature ratios, the use of pressure measurements as an indicator of fully-purged behavior was introduced, and a thermally-driven influence on rim seal performance was quantified.

## NOMENCLATURE

| | |
|---|---|
| b | Hub radius |
| $\dot{m}$ | Mass flow rate |
| P | Pressure |
| PC | Pressure corner |
| PR | Pressure ratio |
| r | Hub radius |
| $s_c$ | Seal clearance |
| t | Time |
| T | Temperature |
| $\alpha$ | Coefficient of thermal expansion |
| $\varepsilon_c$ | Concentration (sealing) effectiveness |
| $\Phi$ | Sealing flow parameter $= \dot{m}_P/(2\pi s_c \rho \Omega b^2)$ |
| $\rho$ | Density |
| $\sigma$ | Radial seal clearance |
| $\tau$ | Blade tip clearance |
| $\Omega$ | Angular velocity |

**Subscripts**

| | |
|---|---|
| 0, 1, 2, A, ... | Measurement locations |
| t0 | Initial condition |
| MGP | Main gas path |
| min | Minimum value to fully purge location C |
| P | Purge flow |
| r | Rotating hardware identifier |
| ref | Reference condition |
| s | Stationary hardware identifier |

## INTRODUCTION

Regardless of application for aircraft propulsion or power generation, gas turbine engines are routinely subject to transient effects. Aircraft engines are required to rapidly transition from idle conditions to provide maximum thrust on-demand for takeoff, and power generation turbines are increasingly expected to perform reliably under hot restart conditions – especially with continuing widespread use of renewable energy sources. Under these transient conditions, gas turbine engines may exhibit compressor surge, blade tip rub events, mechanical interference, and excessive thermal growth leading to relative motion of components away from their design intent. In the turbine section, transient behavior can cause significant impacts on component durability predictions. In particular, critical uncooled underplatform hardware are affected as secondary air streams change due to the nature of the transient and off-design operation of the upstream compressor.

The balance of cooling needs with efficiency debits is an ongoing challenge driving development in the gas turbine industry, and the purge flow that defines rim seal performance is no exception. In recent years, many studies have sought to understand the driving fundamentals of rim seal performance in a steady sense, and some have moved further to evaluate the time-varying behaviors dictating ingress and egress patterns. However, the lack of available data quantifying seal performance due to transient behaviors presents an untapped opportunity for potential improvement over the life of an engine.

The present study uniquely addresses this opportunity by quantifying the effects of purge flow transients on the thermal growth of seal hardware components and corresponding impacts on sealing effectiveness of a stator-rotor seal with an engine-representative design. Furthermore, the use of pressure measurements is extended beyond previous studies implementing similar techniques. Specifically, this study shows that the minimum purge flow required to prevent main gas path ingress applies for rotationally-induced ingress and does not require a prior knowledge of pressure fields or introduction of empirical models.

## LITERATURE REVIEW

The sealing of turbine rims represents a key design parameter required to optimize durability needs with performance targets. Many studies available in the open literature have applied simplified seal geometries to develop a foundational understanding of seal behavior and drive the formation of predictive models. Due to the lack of literature addressing transient seal performance, this review will highlight past research identifying main gas path flow ingestion and connect it with broader transient behaviors relevant to this study.

Fundamentally, rim seal performance can be broken down into two primary mechanisms influencing hot gas ingestion: externally-induced (EI) ingress, rotationally-induced (RI) ingress, and combinations thereof [1-2]. The EI ingress (or egress) represents a pressure-driven effect influenced by a periodic pattern of high and low pressure around the wheel due to the vanes and blades and augmented by a shear layer interaction at the rim seal [3]. Alternatively, RI ingress refers to a disk pumping effect as a result of the rotating disk, through which inward flow occurs adjacent to the stationary hardware to balance outward flow on the opposing rotating components. Owen [4] explains that EI ingress typically dominates seal behavior, but double overlap seal geometries can damp the non-axisymmetric pressure variations causing EI ingress and lead to a dominant RI pattern inboard of the double seal.

Different techniques have been used to experimentally understand ingress and egress patterns. Using carbon dioxide as a tracer gas represents a proven and widely-accepted method for studying sealing effectiveness. $CO_2$ benefits from high light absorption, allowing for higher accuracy from gas analyzers [5]. The relatively high molecular weight does not affect measurement accuracy because flow in the wheelspace is dominated by turbulence [6].

Pressure measurements have also been used to correlate EI ingress and egress trends, particularly for understanding ingress patterns due to pressure non-uniformities [7-8]. More recently, Owen et al. [9] used pressure measurements in combination with an ingress model. These authors identified a so-called “sweet spot,” representing an empirically-determined location on the vane platform upstream of the rim seal. If pressure is measured at this location, it can be used to directly quantify sealing effectiveness for EI ingress.

In addition to understanding the mechanism for ingress, seal clearance can contribute substantially to sealing effectiveness. Bayley and Owen [10] provided an expression for a minimum non-dimensional sealing flow rate as a direct function of non-dimensional axial gap for EI ingress, and Phadke and Owen [11] extended new expressions to more complex geometries, including double seals without overlap.

Using 3D computational fluid dynamics (CFD), Popovic and Hodson [12] showed decreases of radial seal clearance for the outer overlap of a double-overlap rim seal led to improved sealing effectiveness, but with higher sensitivity of pressure loss coefficient with changes in purge flow rate. Furthermore, a change of radial position for rotating and stationary components in the double-overlap geometry (in either direction, outward or inward) showed an improvement of sealing effectiveness in comparison with the baseline position.

Transient effects in turbines have focused primarily on predicting blade tip clearance and its influence on stage performance or mitigation of tip rub events. Kypuros and Melcher [13] developed a model to predict hardware growth due to thermal and rotational effects through transient events and assess tip clearance closedown. Using a state space model, Nielsen et al. [14] explained that pressure effects can be neglected due to their relatively small influence on displacements. Further, the authors showed significant changes in clearance were caused by slow growth rates for the rotor disk relative to adjacent components. Amirante et al. [15] utilized a coupled model of CFD and finite element analysis (FEA) to predict transient temperature effects around knife seals in a low pressure turbine stator well and around a rotor rim seal. This study showed some predictions of rim seal clearance through transient events and emphasized the need to use dynamic meshes in computational simulations due to geometry changes.

Overall, thermal effects are known to cause clearance changes, and these clearance changes have been incorporated into models and computational predictions to develop representative sensitivities. However, thermal growth through transient behavior has not previously been experimentally quantified with correlation to sealing effectiveness through the transient event, as indicated by a lack of public literature. Therefore, this study provides unique insights into overall transient influences on turbine seal performance with engine-representative seal geometries. Using this information, new transient sensitivities can be developed as a function of turbine inlet temperature and identify new methods for assessing a zero ingress condition at locations where the primary mechanism is RI ingress.

## START TURBINE RESEARCH FACILITY

This study was performed in the Steady Thermal Aero Research Turbine (START) Laboratory at The Pennsylvania State University. The START facility (Figure 1) operates in an open-loop continuous-duration mode featuring a one-stage axial turbine test section with hardware representative of the first stage in a modern aero-engine high-pressure turbine. The engine-representative airfoils, cooling architectures, and seal hardware geometries provide a unique insight to the complexity of component performance that may not be adequately captured by simplified geometries. A brief explanation of the facility is summarized here, and further details are provided by Barringer et al. [16] and Berdanier et al. [17].

A continuous pressurized air supply for the turbine is provided by two identical 1.1 MW (1500 hp) industrial compressors outputting 5.7 kg/s (12.5 lbm/s) at a nominal design point of 480 kPa and 383K (70 psia and 230°F). Together, up to 10.4 kg/s (25 lbm/s) of air is available for use. A 3.5 MW in-line natural gas heater was designed to offer main gas path (MGP) temperatures up to 675K (750°F) at the full combined flow rate.

A portion of the pressurized air (approximately 10% of the total supply flow rate) is redirected through a shell-and-tube heat exchanger with continuous operating capability down to 273K (32°F). This cooled air is directed to several independently controlled flow lines that distribute cooling air throughout the turbine test section. Each of these lines incorporates a dedicated Venturi meter to measure flow rate. To align with measurements from previous studies, tangential on-board injection (TOBI) flow was not introduced for this study. Therefore, the present study focuses only on effects related to the purge hole flow (identified in Figure 2). Nonetheless, the illustration in Figure 3 shows some purge air may make its way through the cooling holes in the blades due to the pressure difference between the underplatform region and the MGP, as described by Berdanier et al. [17].

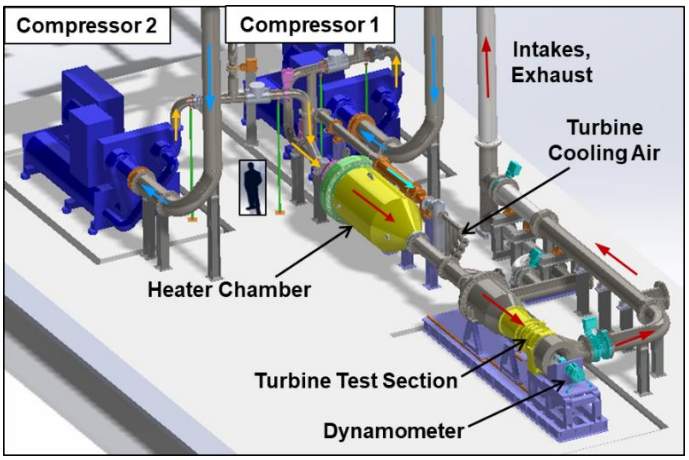


**Figure 1. START turbine research facility layout.**

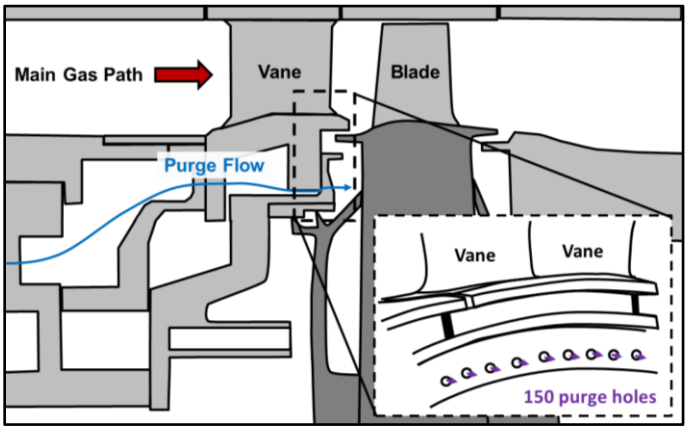


**Figure 2. Turbine flowpath identifying purge flow holes.**

The purge flow is fed from a plenum under the platform of the first stage vane (1V) that leads to the vane-blade cavity through 150 identical equally-spaced purge holes, as outlined by Clark et al. [18] and Berdanier et al. [17]. The purge flow rate is set by a remotely-actuated valve, and the time constant representing a change from fully-closed to fully-open (or vice-versa) is approximately 90 seconds.

The turbine power is extracted through a water brake dynamometer with an operating range up to 1200 hp at 11,000 rpm. The measurements presented in this study focused on an operating condition at 9,500 rpm with a typical variability of ±10 rpm or better. Other relevant operating conditions are outlined in Table 1.

**Table 1. Turbine Operating Conditions for Low-Temperature Setpoints**

| Parameter | Value |
|---|---|
| Density ratio, $\rho_P/\rho_{MGP}$ | 1.1 – 1.5 |
| Vane inlet Mach number | 0.1 |
| Vane inlet axial Reynolds number | $1 \times 10^5$ |
| Blade inlet axial Reynolds number | $1.4 \times 10^5$ |
| Rotational Reynolds number | $3.5 – 6.0 \times 10^6$ |

### Facility Instrumentation and Measurements

A schematic of test section instrumentation pertinent to this study is outlined in Figure 3. Fixed Kiel head total pressure probes and thermocouple probes distributed circumferentially around the annulus define the MGP inlet conditions approximately eight axial chords upstream of the vane leading edge. Assessment of seal performance is quantified by measurements from static pressure taps and thermocouples positioned throughout the stationary underplatform hardware.

A few of the engine vanes were replaced with direct metal laser sintered (DMLS) nickel alloy vanes. These additively manufactured components leverage the ability to embed pressure channels through the vane to create static pressure taps on the wetted surface in the MGP and in the rim seal region. For pressure and temperature sensors alike, a series of sensors (four or more) at each identified location in Figure 3 are distributed

around the circumference to develop a representative average at each location. The static pressure taps provide dual functionality through the ability to measure pressure directly, but also extract and redirect flow through a gas analyzer for $CO_2$ tracer gas analyses to quantify sealing effectiveness.

Real-time rotor blade tip clearance measurements were collected from four capacitive tip clearance sensors equally spaced around the circumference and operated by a frequency modulated (FM) principle. The sensors were designed and installed in a manner that ensures the probe faces are positioned consistently with respect to the inner diameter of the rotor casing, including periods of thermal growth and transient events. Details of a similar system are outlined by Berdanier and Key [19] with considerations for component-level uncertainty contributions.

Facility measurements from all sensors were collected continuously and averaged over subsequent one second intervals for an effective recording rate of 1 Hz. To ensure measurement performance through transient periods, short small-diameter pressure tubing ensured a settling time for pressure measurements much less than the recording rate, and small gauge thermocouple wires were used to reduce thermal lag effects. The thermocouple beads installed at locations $T_1$ and $T_2$ measure fluid temperature very near the surface; the thermocouple at location $T_3$ is in direct contact with the surface.

A complete uncertainty analysis was performed for this study, and uncertainty of calculated parameters was determined following the partial differential root-sum-squares method outlined by Figliola and Beasley [20]. Using this approach, representative uncertainties for relevant parameters are included in Table 2, for which the reference conditions denote the maximum capability of the facility outlined in the previous section. The values reported in Table 2 represent a total combination of bias and precision uncertainty. For reported steady measurements, the contribution of precision uncertainty was further minimized by calculating an average of data collected over a 30-second window of steady operation.

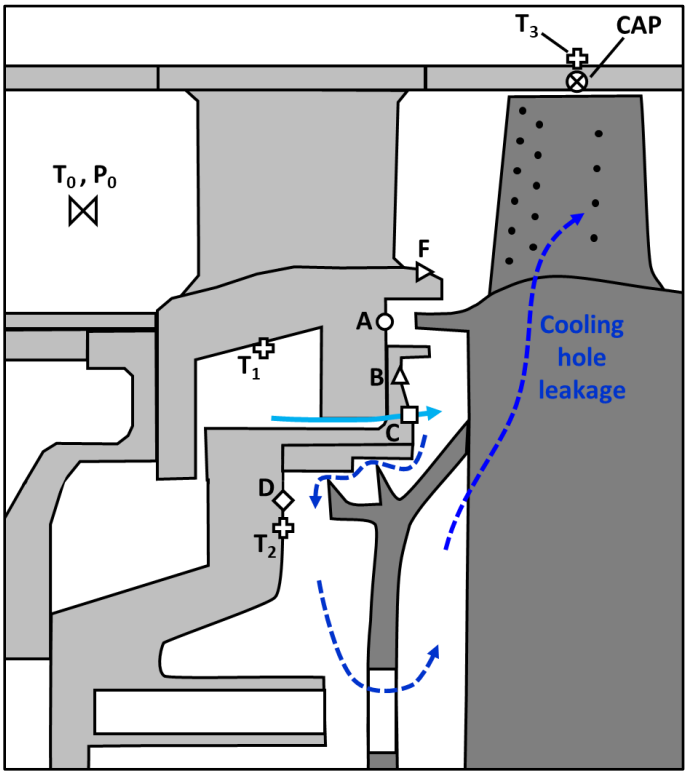


**Figure 3. Relevant test section instrumentation layout.**

**Table 2. Uncertainty of Relevant Turbine Measurements**

| Parameter | Total Uncertainty |
|---|---|
| Main gas path flow rate, $\dot{m}_{MGP}/\dot{m}_{MGP,ref}$ | ± 0.0040 |
| Pressures, $P/P_{ref}$ | ± 0.0010 |
| Temperatures, $T/T_{ref}$ | ± 0.0006 |
| Purge flow rate, $\dot{m}_P/\dot{m}_{P,ref}$ | ± 0.0180 |
| Sealing effectiveness, $\varepsilon_c$ | ± 0.0250 |
| Rotor tip clearance, $\tau/r_s$ | ± 0.0001 |

## TRANSIENT TURBINE OPERATION

For initial consideration of transient effects, the MGP conditions were set for a low-temperature main gas path without heat addition from the in-line heater (383K, 230°F). To achieve the desired transient purge flow conditions, a series of steps were performed, as indicated in Table 3 and Figure 4. In Figure 4, the entire 1 Hz data series is reported, and one data point is superimposed as a marker every two minutes through the transient event. A detailed view of period (i) is presented in Figure 5 to further characterize the valve behavior and the corresponding change of purge flow rate as a function of time. In Figure 5, representative data points are provided as markers in 10 second intervals.

For these figures and throughout the paper, the purge mass flow rate, $\dot{m}_P$, is nondimensionalized by $\dot{m}_{P,min}$, the minimum purge mass flow rate required to purge the rim cavity at location C in Figure 3. In this case, the nondimensional relationships presented by $\dot{m}_P/\dot{m}_{P,min}$ are analogous to the relationships of normalized nondimensional sealing parameter, $\Phi/\Phi_{min}$, often utilized in model-based studies (e.g., Owen [4]).

As shown in Figure 4, the turbine was first allowed to thermally soak at the desired operating condition with zero purge flow. Next, the purge flow control valve was set to a fully-open setpoint, and the valve steadily opened over a 90 second duration, as outlined in the previous section; this transient period will be identified as (i). Once the full-flow purge condition was achieved, the test section was allowed to thermally soak (as defined by a temperature gradient less than 0.06 K/min measured by sensor $T_2$); this thermal soak period is identified by (ii). Finally, the valve setpoint was adjusted to by fully closed, and the valve steadily moved until the zero purge condition was again achieved; this period is identified by (iii). A fourth period, (iv),

represents the thermal soak process with zero purge flow. By passing through each of these subsequent periods, a full transient "loop" can be performed, ultimately returning to the original starting point for the system.

**Table 3. Transient Operating Periods**

| Period | Description |
|---|---|
| (i) | Increasing purge flow |
| (ii) | Thermal soak at high purge flow |
| (iii) | Decreasing purge flow |
| (iv) | Thermal soak at zero purge flow |

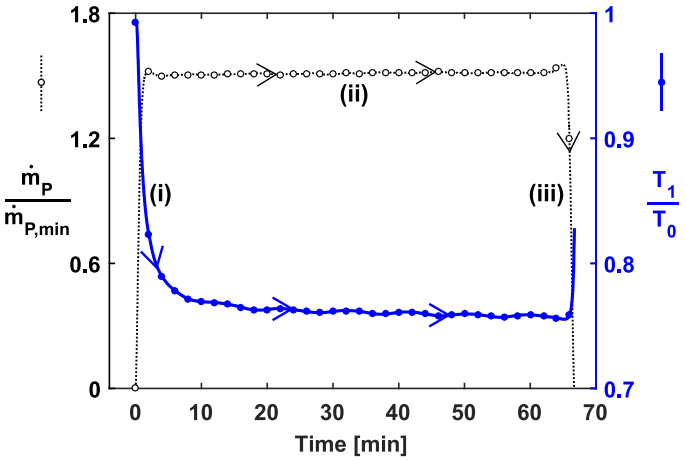


**Figure 4. Temporal change of purge flow and underplatform hardware temperature through transient purge flow process periods (i)-(iii). For clarity, data collected at 1 Hz, are represented by markers spaced two minutes apart.**

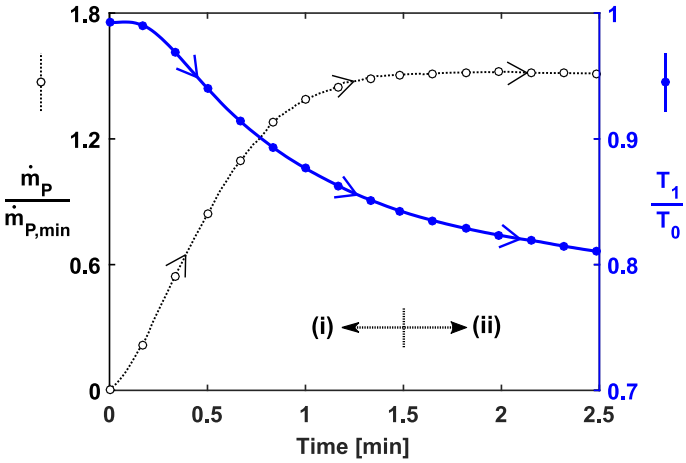


**Figure 5. Focus on purge flow transient period (i) from Figure 4 characterizing valve behavior. Markers are spaced 10 seconds apart.**

## Thermal Growth Considerations

As the underplatform hardware changes temperature with the modulation of purge flow in Figure 4, a thermal growth effect is expected. Although the test section is highly instrumented, direct measurement of temperatures in the rim seal region were not collected. Instead, the measured temperature $T_1$ is used as a representative approximation of the stationary hardware in the rim seal region. Further justification for the use of $T_1$ as an indicator of rim seal hardware temperature follows in subsequent discussion. The temperature $T_1$ in Figure 3 is shown as a function of purge mass flow rate in Figure 6, and a series of steady thermally-soaked temperature measurements are also shown for comparison. These data were collected by allowing the underplatform hardware to reach thermal steady-state after each incremental increase in purge flow rate. A linear expansion principle was applied to estimate the thermal expansion of the stationary rim seal radius identified in Figure 7:

$$\Delta r_s = r_{s,t0}\, \alpha\, \Delta T\,, \tag{1}$$

where $r_{s,t0}$ is the initial radius of the stationary hardware, $\alpha$ is the coefficient of thermal expansion, and $\Delta T$ is the measured temperature change. For the present study, the underplatform hardware components are manufactured from 410 stainless steel, and a fixed coefficient of thermal expansion representative of the temperature range of interest was applied using material properties from Harvey [21]:

$$\alpha = 11\times10^{-6}\ \text{m/m-K}\,. \tag{2}$$

Through Equations (1) and (2), the measured temperature data $T_1$ presented on the left ordinate in Figure 6 are simultaneously referred as a dimensional change on the right ordinate based on a uniform temperature assumption. As shown in Figure 6, the introduction of purge flow in period (i) yields an immediate decrease of temperature, $T_1$, and a corresponding thermal growth effect. The circuitous path of purge flow through the underplatform geometry necessitates that these hardware components are fully coated by the cool air, and the convection dictates a short time response for the temperature measurements. In contrast, the reduction of purge flow in period (iii) drives a slower time response as the underplatform temperature increase is driven instead by conduction through the hardware from the hot main gas path.

With this knowledge of thermal growth effects on the stationary seal geometry, the rotating geometry must be evaluated separately to fully understand the transient effects on the radial seal clearances. To address this need, the real time rotor tip clearance measurements provide a valuable insight. Because the transient purge flow effect is primarily driven by impingement of cooling air on the disk and operating speed was maintained (i.e., no centrifugal blade growth), using blade tip clearance as an indicator of seal geometry changes represents a valuable approximation.

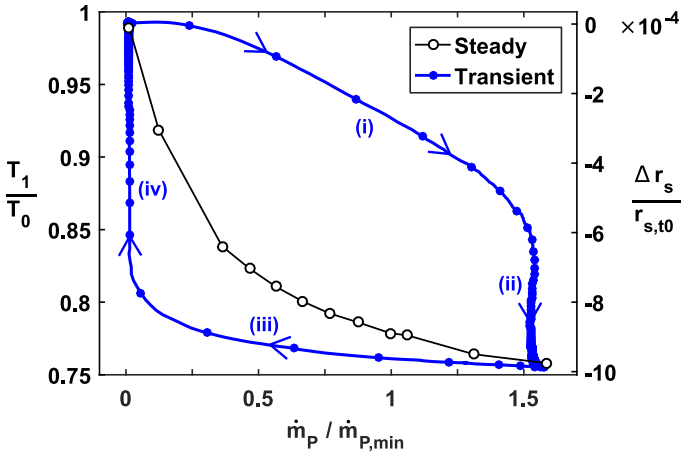


**Figure 6. Measured underplatform hardware temperature and thermal growth as a function of purge flow rate through transient process. Transient data markers are spaced 10 seconds apart.**

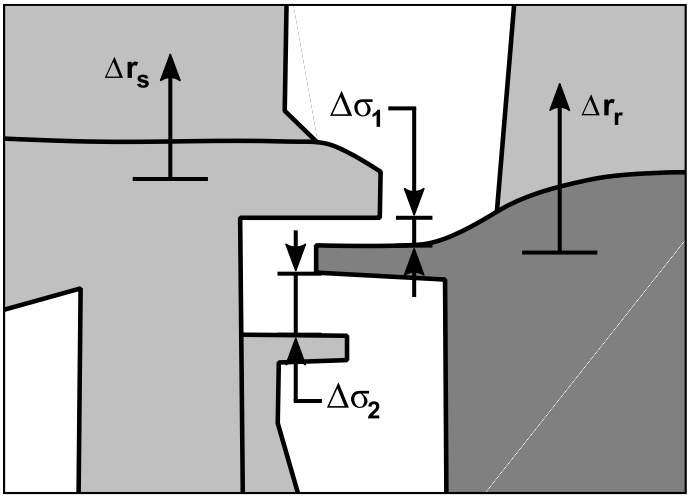


**Figure 7. Illustration of underplatform hardware identifying thermal growth for stationary and rotating components.**

In this case, the direct influence of blade and disk growth on seal performance is limited to radial locations inboard of the blade hub; blade growth within the main gas path is not a driver of seal geometry change, but would be measured by the tip clearance probes. Although this blade growth in the main gas path cannot be directly separated from the growth of the disk and root, the maintenance of a fixed MGP inlet temperature dictates that it is a second-order effect. For further verification, however, it is possible to quantify changes due to thermal growth of the casing itself. Using rotor casing surface temperature measurements ($T_3$ in Figure 3), the temperature change through the purge flow transient was less than 0.8 K, which correlates to a nondimensional radius change, $\Delta r_s / r_{s,t0}$ less than $1\times10^{-5}$ using Equation (1), and is not a significant contributor relative to the results in Figure 6.

All radial changes of dimension due to thermal growth are defined to be positive. As shown in Figure 7, decreases of blade tip clearance, $\tau$, correlate to an outward radial growth of blade and disk hardware and, therefore, represent a one-for-one positive increase of seal radius on the rotating hardware, $r_r$:

$$\Delta r_r \approx -\Delta\tau \,. \tag{3}$$

Experimentally measured changes of rotor tip clearance through the transient process are shown in Figure 8, with an overlay of the data series collected under thermally steady conditions. In contrast to the response of the stationary hardware in Figure 6, Figure 8 shows a slow time response of tip clearance change as purge flow is introduced. In fact, the tip clearance is nearly constant across the period of increasing purge flow, (i). Here, the change of tip clearance occurs almost exclusively during the thermal-soaking period, (ii). The reasons for this trend are twofold: first, the impingement of purge flow on the rotor hardware occurs over a relatively small area; second, a distribution of cooling air over the disk requires a path around the coverplate and through the entry holes reserved for TOBI nozzle flow (recall here that no TOBI flow was included in this study). Understandably, some cooling flow makes its way around the coverplates and into the blades themselves, as shown by the dashed line in Figure 3. However, it is still the primary responsibility of conduction through the coverplates to the disk to facilitate the thermal growth process – a relatively slower influence than the direct forced convection identified in Figure 6. The decrease of purge flow, period (iii) yields a clearance change that is similar in magnitude to period (i), further supporting this behavior.

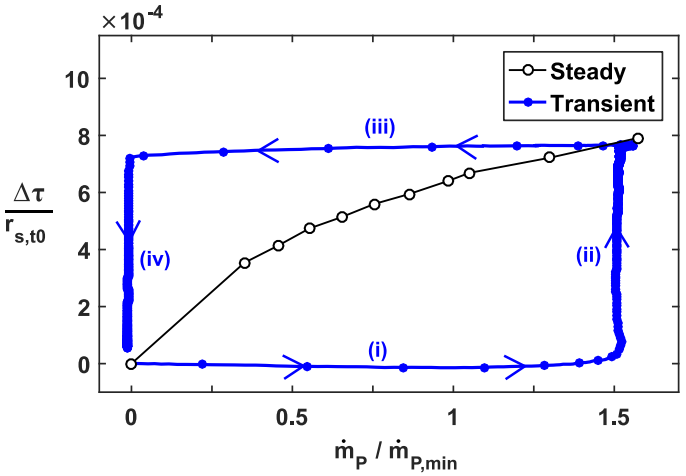


**Figure 8. Measured rotor blade tip clearance change through transient events. Transient data markers are spaced 10 seconds apart.**

Referring back to the illustration in Figure 7, the stator-rotor seal clearances in the double-overlap seal configuration are identified by $\sigma_1$ and $\sigma_2$ for the outer and inner clearances, respectively. Using these definitions, the seal clearance changes are evaluated using the relative contributions from stationary and

rotating sides of the seal. The double-overlap seal design dictates that the changes of these two seal clearances, $\sigma_1$ and $\sigma_2$, exhibit a direct negative correlation:

$$\Delta\sigma_1 \approx \Delta r_s - \Delta r_r$$
$$\Delta\sigma_2 \approx -\Delta\sigma_1 \approx \Delta r_r - \Delta r_s \,. \quad (4)$$

Through the convention outlined in Equation (4), an approximation of the transient rim seal clearance change for the outboard gap, $\Delta\sigma_1$, is presented in Figure 9. Two data series are shown in Figure 9. The first represents $\Delta\sigma_1$ as a function of the measured temperature, $T_1$ (i.e., using the temperature traces shown in Figure 6). As an alternative, a relationship similar to Figure 6 could also be created using $T_2$, and the corresponding seal clearance changes are also shown in Figure 9. Beginning with Figure 9 and continuing for the remainder of this paper, regularly-spaced data points are omitted from the transient data traces to reduce figure complexity.

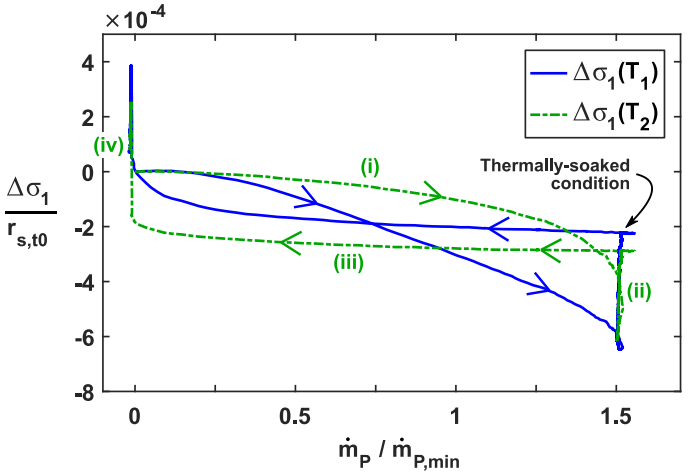


**Figure 9. Measured transient seal clearance change as a function of relative purge flow rate for two different temperatures.**

A few critical observations are identified between the two data series in Figure 9. First, the use of $T_1$ identifies a faster time response through period (i) due to the location of the sensor on hardware with wetted surface area benefitting from convection by the cooling air. In contrast, $T_2$ is in a location that is influenced by conduction through the underplatform hardware and the migration of cool purge flow air throughout the stator-rotor cavity. Despite the different temporal trends calculated from $T_1$ and $T_2$ in Figure 9, the minimum nondimensional seal clearance change, $\Delta\sigma_1/r_{s,t0}$, for the two curves differs by only $3\times10^{-5}$ (achieved at a full-flow purge condition).

More precisely, the change of outer seal clearance, $\Delta\sigma_1$, is likely represented by a behavior somewhere between the two curves in Figure 9. Regardless of the differences, the qualitative conclusions applicable to the outer seal clearance, $\sigma_1$, drawn from Figure 9 are consistent: (1) the minimum seal clearance occurs near the end of transient phase (i); (2) the seal clearance grows throughout the thermal soak phase (ii); (3) the non-dimensional thermally-soaked seal clearance with full-flow purge is approximately $2\times10^{-4}$ less than the seal clearance with zero purge flow; (4) the thermal lag associated with the rotating components dictates a maximum seal clearance achieved near the end of transient phase (iii); (5) the hardware returns to its original state at the end of phase (iv).

## TRANSIENT STATOR-ROTOR SEAL PERFORMANCE

In addition to the thermal growth effects associated with transient purge flow changes previously shown, the implication of those transient effects on the performance of the stator-rotor seal were evaluated. Previous measurements presented by Berdanier et al. [17] assessed stator-rotor seal performance for these same geometry and operating conditions. In that study, $CO_2$ was used as a tracer gas to quantify concentration effectiveness, which is a direct indicator of sealing:

$$\varepsilon_c = (c - c_\infty)/(c_s - c_\infty)\,. \quad (5)$$

By this equation, the concentration effectiveness is a parameter in the range of zero to one representing the ratio of the difference between $CO_2$ concentration measured at a given location, c, and the background level, $c_\infty$, to the difference of the supply concentration, $c_s$, and the background level. When injecting a known amount of $CO_2$ into the purge flow, a low concentration effectiveness represents a majority of hot (MGP) air, whereas a high concentration effectiveness represents a majority of cool (purge) air. Further details outlining the use of $CO_2$ as a tracer gas are outlined by Clark et al. [18,22].

The steady results of sealing effectiveness from Berdanier et al. [17] are presented in Figure 10 over a range of relative purge flow rates. These steady data represent the same operating conditions, including 383K inlet temperature.

Initial attempts to quantify time-resolved sealing effectiveness through the transient event using $CO_2$ as a tracer

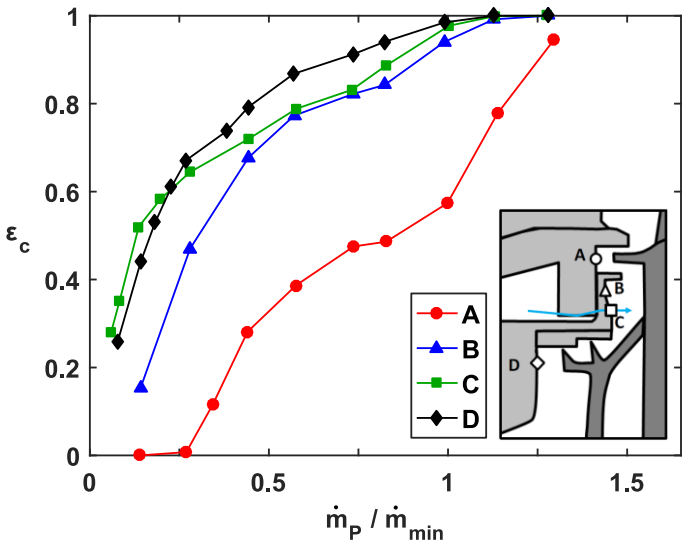


**Figure 10. Steady sealing effectiveness trends as a function of relative purge flow rate at several positions in the seal cavity.**

gas were challenged by recovery times required by the gas analyzer system. However, short pressure tubes facilitated time-resolved pressure measurements. Specifically, the settling time was calculated to be approximately 40 ms, which was much less than the data acquisition sampling rate (1 Hz) or the time scale of the transient behavior shown in Figure 5. As a result, the static pressure measurements are able to adequately capture the transient conditions in the underplatform region.

Initially, measurements in the rim seal position (A in Figure 3) were evaluated through the transient process as a function of relative purge flow rate as shown in Figure 11. In Figure 11, the rim seal pressure is represented by a nondimensional pressure ratio difference with respect to the initial condition at the beginning of period (i) in the transient:

$$\Delta PR_{A-0} = PR_{A-0} - PR_{A-0,t0}\,, \tag{6}$$

where the pressure ratio $PR_{A-0}$ is a function of the dimensional rim seal static pressure, $P_A$, and the turbine inlet total pressure, $P_0$:

$$PR_{A-0} = P_A / P_0\,. \tag{7}$$

In addition to the transient data, Figure 11 also includes a comparison with the steady thermally-soaked operating points over a similar range of relative purge flow rates. For these steady measurements, the same initial condition was subtracted (i.e., Equation (6)) to ensure a direct comparison with the transient data.

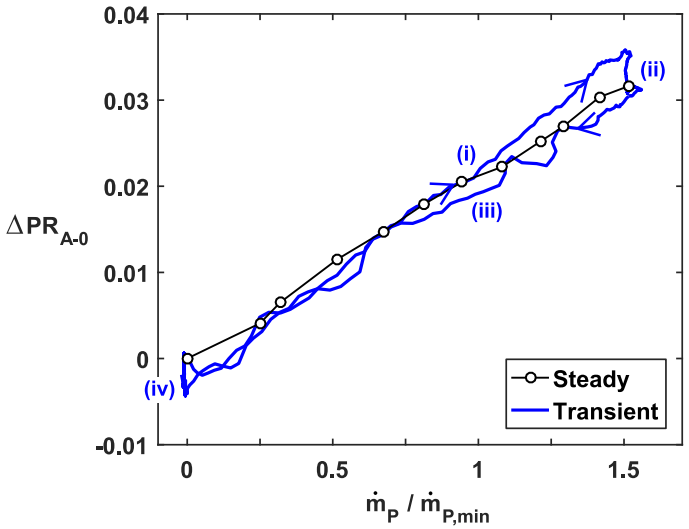


**Figure 11. Measured difference of pressure ratio with respect to turbine inlet through transient events for rim seal location A.**

The rim seal pressure data in Figure 11 show a transient path that is nearly repeatable in the range of nondimensional purge flow rates less than unity. For nondimensional purge flow rates greater than one, there is a slight divergence of the paths defined by periods (i) and (iii). Referring back to Figure 9, the temperature curve defined by $\sigma_1(T_2)$ shows a nondimensional seal clearance which decreases more rapidly for nondimensional purge flow rates greater than unity in period (i). In contrast, the duration of period (iii) shows a nondimensional seal clearance that is approximately constant across the entire range of purge flow rates, which agrees with the trend in Figure 11 that approximately follows the steady data points. This observation begins to suggest that the underplatform temperature $T_2$ may be a better indicator of rim seal clearance. Further evaluation of the transient data in Figure 11 also shows an apparent "wobble" in the path for period (iii). This pattern supports an understanding of highly unsteady behavior in the outboard locations driven primarily by EI ingress.

Beyond the rim seal location, the inboard rim cavity location (C in Figure 3) is presented using a similar pressure ratio based on MGP turbine inlet total pressure given in Figure 12. In contrast with the rim seal measurements, the inboard measurements in Figure 12 show a distinct hysteresis pattern separating periods (i) and (iii), with the steady data points positioned somewhere between.

Although not shown here, a similar hysteresis pattern is present for the outer rim cavity location B and the innermost location D. With this knowledge, a comparison of Figure 11 and Figure 12 leads to several key observations. First, a separation can be made between the behavior of the outboard location A from the inner positions B, C, and D. Recalling these locations in the context of the overall seal geometry, as seen in Figure 3, this demarcation is a result of the double-overlap seal configuration, through which the inner overlap drives a different seal performance. Specifically, the inner overlap acts as an interference, effectively damping the inner measurement locations from the main gas path and rim seal regions. This conclusion dictates EI ingress at location A versus rotationally-induced (RI) ingress at locations B, C, and D [4]. Ultimately, both seal clearances in the double overlap seal geometry drive the pressure hysteresis observed in the inner wheel-space region.

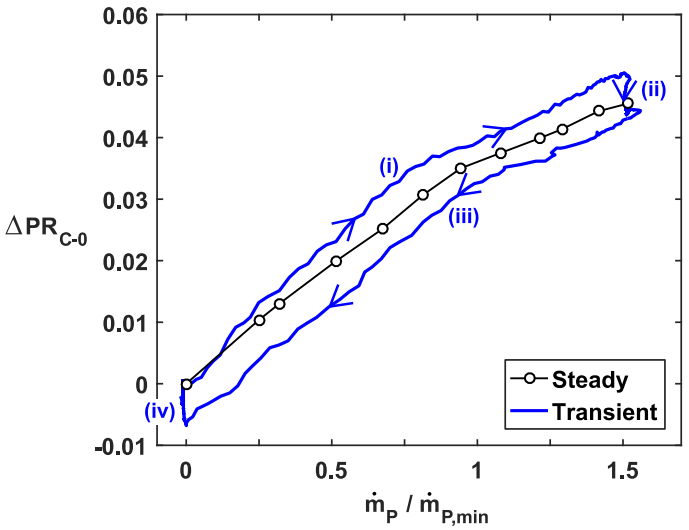


**Figure 12. Measured difference of pressure ratio with respect to turbine inlet through transient events for rim seal location C.**

Thus far, a transient hysteresis has been identified in pressure measurements, and there is an expectation that a similar influence may exist for the transient sealing effectiveness. To help address this, a different pressure representation was constructed. In this new formulation, the pressure ratio across the seal was considered, using the pressure at the inner diameter of the main gas path near the mouth of the seal as the reference condition, location F. Following the procedure outlined in Equations (6) and (7), a pressure difference is defined with respect to the initial conditions at the start of transient period (i):

$$\Delta PR_{C-F} = PR_{C-F} - PR_{C-F,t0}\,, \tag{8}$$

where the pressure ratio $PR_{C-F}$ is a function of the dimensional rim cavity static pressure, $P_C$, and the vane hub trailing edge measurement, $P_F$ (see Figure 3):

$$PR_{C-F} = P_C \,/\, P_F\,. \tag{9}$$

The nondimensional pressure is presented using these definitions in Figure 13. However, with knowledge that the hysteresis in pressure measurements for inboard locations is caused by thermal transient effects, additional tests were conducted to assess the influence of MGP inlet temperature excursions with a fixed cooling flow temperature. A comparison is shown in Figure 13 for two temperature extremes, 383 K (the inlet condition for all measurements shown thus far) and 416 K.

Recasting the location C rim cavity pressures using Equation (9) shows a plateau that is achieved for high values of purge flow, with a relatively sharp corner present in the transient hysteresis and the steady data points. The presence of this gradient change and the corresponding "pressure corner" (PC) was previously identified by Berdanier et al. [17] for configurations with and without blade cooling holes, so its development is not a result of the flow leakage through the blade cooling holes. A comparison of Figure 13 with Figure 12 shows a similar but less pronounced feature identifiable in Figure 12, highlighting the value of the pressure ratio definition in Equation (9). Further evaluation of the different temperature series in Figure 13 points to a changing behavior of the "pressure corner" and subsequent plateau.

At this point, a question remains regarding the cause of these patterns. To answer this question, the nondimensional pressure change from Figure 13 is superimposed with the steady $CO_2$-based sealing effectiveness measurements for location C from Figure 10. The connection of these data, shown in Figure 14, indicates that the PC location for the steady data coincides with the minimum purge flow condition at which a fully-purged cavity is identified by the $CO_2$ concentration effectiveness measurements, $\dot{m}_{P,min}$ (typically represented by $\varepsilon_c > 0.95$ [2]). Based on this, the identified pressure plateau exists when the measurement location exhibits fully-purged behavior.

In Figure 14, the PC location for the decreasing transient period (iii) occurs at the same relative purge flow rate as the steady data, indicating that the fully-purged condition is maintained between those two cases. Also in Figure 14, the steady and unsteady curves follow the same path at higher purge flow rates because there is no ingestion of high temperature MGP air to drive heat transfer to the underplatform hardware. When the purge flow rate decreases past the PC in transient period (iii), the steady and transient curves diverge as hot MGP flow begins to enter the underplatform cavity. This observation also aligns with the predicted seal clearance behavior in Figure 9. Specifically, seal clearance changes occur more rapidly in transient period (i) than in transient period (iii), as reflected in Figure 14 by the rate of divergence of the steady and transient curves in these periods. Because seal clearances change more quickly in transient period (i) (driven by high ingestion of hot MGP air), the steady and transient curves diverge more rapidly when compared to the divergence in transient region (iii).

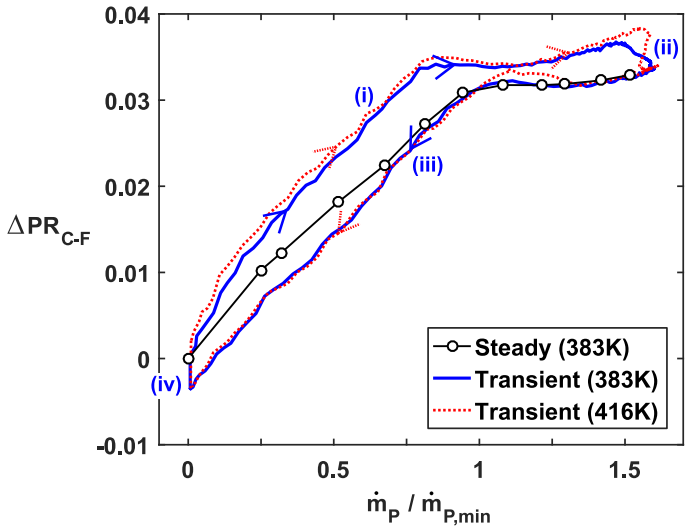


**Figure 13. Measured difference of pressure ratio across seal for location C at two MGP turbine inlet temperatures.**

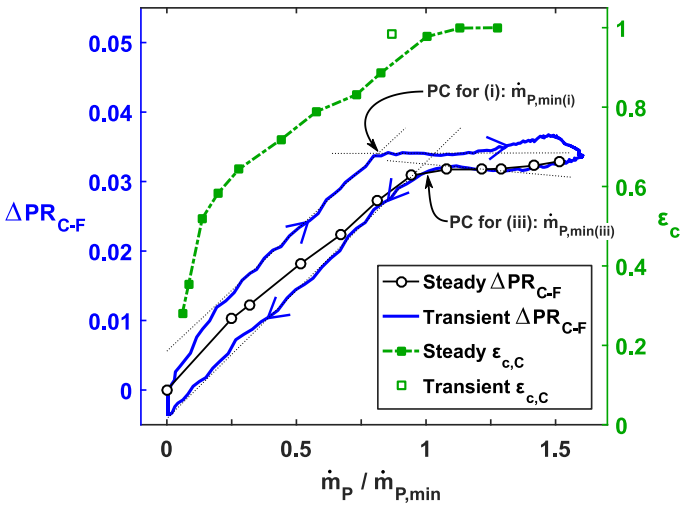


**Figure 14. Measured difference of pressure ratio across seal for location C with sealing effectiveness measurements at the same location.**

When examining the period of increasing purge flow (i), the PC location occurs at a noticeably lower relative purge flow rate, indicating a fully-purged seal at a lower purge flow rate than the steady condition. This also agrees with expectations from the predicted seal clearances in Figure 9, as the fast temperature response yields a corresponding fast thermal growth of the stationary hardware components leading to a transient closedown of the seal gap.

To further support these observations, concentration effectiveness measurements were collected using $CO_2$ tracer gas at a purge flow rate near the PC identified for the increasing transient period (i). Beginning from a steady, thermally-soaked operating condition, the purge flow rate was increased at the same rate, but stopped at the target point. This purge flow transient event is shown in Figure 15. Because the valve was stopped at a point in the middle of its stroke, there is no gradual change of temporal purge flow rate gradient, $d\dot{m}_P/dt$, as the set point is approached (in contrast to the fully-opened behavior characterized in Figure 5, which exhibited a decreasing $d\dot{m}_P/dt$ roll-off at the end of the valve stroke).

The injected $CO_2$ concentration required to maximize the sensor range and achieve desired resolution at high purge flow rates is greater than what is required at low flow rates. As a result, the output from the gas analyzer is initially out of range when the transient event begins through period (i). As the purge flow rate increases and ultimately reaches the desired purge flow setpoint (time t=0 in Figure 15), the gas analyzer recovers from the overrange condition. After this recovery period (about 20 seconds for these conditions, which includes a characterized gas analyzer time delay of approximately 12 seconds), a decay of sealing effectiveness is observed in Figure 15 associated with the thermal growth of the hardware components. Throughout the thermal soak period associated with the steady purge flow rate (t>0 in Figure 15), the sealing effectiveness decays to a final value slightly less than 0.94, which agrees with the steady sealing effectiveness data series in Figure 14 at the selected purge flow rate. To determine the representative transient sealing effectiveness, an exponential fit was applied to the decaying data and extrapolated through the recovery period back to t=0. This endpoint, identified by the open marker in Figure 15 represents the same open marker for sealing effectiveness in Figure 14. The transient data marker in Figure 14 highlights the shift of sealing effectiveness due to thermal effects associated with transient events and validates the utility of pressure measurements as an indicator of fully-sealed seal performance.

Equipped with a validated method for identifying fully-purged seal performance, the reduction of purge flow rate required to fully-purge the rim cavity position C was evaluated. The exact PC position was determined through an intersection of two linear fits (one for the plateau adjacent to the PC and another for the increasing/decreasing segment). In this way, human interpretation was removed from the PC identification process. These fully-purged flow rates are identified in Figure 14 as $\dot{m}_{P,min(i)}$ and $\dot{m}_{P,min(iii)}$ for the increasing period (i) and decreasing period (iii), respectively. Therefore, the reduction of purge flow rate required to fully purge the cavity through transient purge flow events is calculated according to:

$$\Delta\dot{m}_{P,min} = \frac{\dot{m}_{P,min(iii)} - \dot{m}_{P,min(i)}}{\dot{m}_{P,min(iii)}} \times 100\% \,. \qquad (10)$$

This fully-sealed purge flow rate reduction, $\Delta\dot{m}_{P,min}$, is represented by percentage reduction from the period (iii) value (also equal to the steady thermally-soaked value). An application of Equation (10) to transient pressure data collected at three MGP temperatures (with fixed purge flow temperature) yields the results shown in Figure 16.

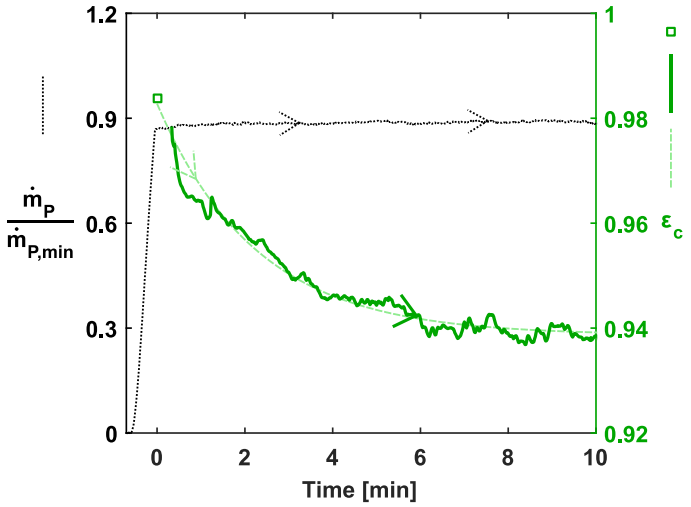


**Figure 15. Measured decay of sealing effectiveness at location C immediately following increasing purge flow rate transient.**

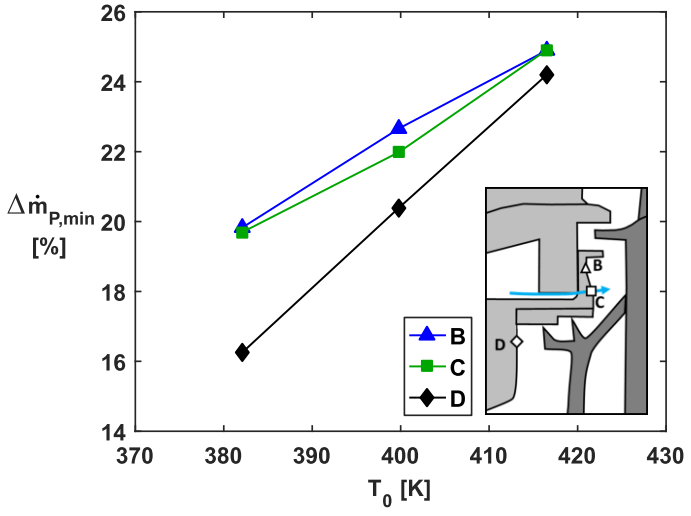


**Figure 16. Change of fully-purged flow rate at different rim cavity locations through transient process for different MGP turbine inlet temperatures.**

Over the assessed temperature range, increases of MGP turbine inlet temperature correspond to increasing differences of fully-sealed purge flow as the thermal growth effects become increasingly influential. The close proximity of the two rim cavity positions, B and C, justifies their nearly identical patterns (both in absolute value and gradient) with increasing MGP temperature. The relative distance from location D to the hot main gas path and the slightly higher base values of sealing effectiveness (Figure 10) contributes to lower changes and a steeper gradient in Figure 16. Understandably, because the trends in Figure 16 are driven by thermal growth effects, the absolute values will be significantly influenced by parameters such as absolute purge flow rate, air temperatures (MGP and secondary cooling air), and purge flow ramp rate.

## SUMMARY AND CONCLUSIONS

This study utilized a one-stage turbine with engine-representative hardware to assess transient purge flow behavior and its impact on stator-rotor seal performance. The continuous-duration operating mode of the START research turbine facility is ideal for evaluating transient effects due to its ability to ramp through a specified operating variable and elicit behavior such as thermal growth effects. The measurements collected in this study were outlined to identify general trends associated with transient events in a full-scale engine.

Using simple linear expansion principles, measured temperatures were used to calculate thermal growth of the stationary underplatform hardware representing the stationary side of the stator-rotor seal geometry. Rotor blade tip clearance measurements validated the estimations of thermal growth associated with the rotating side of the stator-rotor seal. Ultimately, a considerable thermal lag was identified for the rotating hardware, driven primarily by a limited area of impingement cooling from the purge holes and a substantial thermal mass associated with the rotor disk. Furthermore, different trends were quantified for the cases of increasing purge flow and decreasing purge flow (primarily influenced by forced convective cooling and conductive heating from the main gas path, respectively).

With a preliminary understanding of thermal growth associated with transient processes, the performance of the double-overlap seal geometry was evaluated using a combination of static pressure measurements distributed throughout the rim seal, rim cavity, and front wheelspace areas. Further validation of the results was provided by concentration effectiveness measurements quantifying sealing performance using a tracer gas sampled through the same static pressure taps.

The pressure measurements collected through the transient purge flow events showed little hysteresis in the outermost rim seal location, whereas significant hysteresis was observed at the locations inboard of the second overlap in the double-overlap seal geometry. Furthermore, observations suggest the double-overlap design sufficiently damps effects from externally-induced ingress, leaving the inboard measurement locations to be dictated by rotationally-induced behaviors.

Through a comparison with $CO_2$-based sealing effectiveness measurements, the use of a pressure ratio across the seal was demonstrated as a viable method for identifying the minimum purge flow required to fully seal a given measurement location if the position of interest is governed by rotationally-induced (versus externally-induced) mechanisms, even under transient conditions. In comparison with tracer gas techniques, pressure measurements are simpler and more cost effective, particularly through simultaneous measurement capability from many channels. As a result, using pressure measurements to identify fully-sealed behavior offers a potential for quick assessment of novel seal geometries and provides an opportunity for entry with engine platforms.

Finally, the pressure measurement technique suggested by this study for identifying fully-sealed behavior was applied to quantify a seal performance improvement associated with the transient purge flow process. A linear trend was identified at all inboard measurement locations, showing a 20 percent decrease of relative purge flow is possible through the transient events evaluated in this study.

This study suggests new techniques through which sealing effectiveness may be quantified for stator-rotor cavities, and begins to evaluate the potential impact of relevant transient behaviors in axial turbines. The ability to quantify these potential performance debits (or merits) as an integral part of hardware design and lifing models is particularly relevant for next-generation engine designs desensitized to transient events.

## ACKNOWLEDGMENTS

This material is based upon work supported by the Department of Energy under Award Number DE-FE0031288. The authors would also like to recognize and thank Pratt & Whitney for supporting research presented in this paper. This report was prepared as an account of work sponsored by an agency of the United States Government. Neither the United States Government nor any agency thereof, nor any of their employees, makes any warranty, express or implied, or assumes any legal liability or responsibility for the accuracy, completeness, or usefulness of any information, apparatus, product, or process disclosed, or represents that its use would not infringe privately owned rights. Reference herein to any specific commercial product, process, or service by trade name, trademark, manufacturer, or otherwise does not necessarily constitute or imply its endorsement, recommendation, or favoring by the United States Government or any agency thereof. The views and opinions of authors expressed herein do not necessarily state or reflect those of the United States Government or any agency thereof.

## REFERENCES

[1] Johnson, B. V., Mack, G. J., Paolillo, R. E. and Daniels, W. A., 1994, "Turbine Rim Seal Gas Path Flow Ingestion Mechanisms," AIAA Paper No. 94-2703, Indianapolis, Indiana, USA.

[2] Scobie, J. A., Sangan, C. M., Owen J. M., and Lock G. D., 2016, "Review of Ingress in Gas Turbines," *ASME J. Eng. Gas Turb. Power*, **138**(12), p. 120801.
[3] Savov, S.S. and Atkins, N.R., 2017, "A Rim Seal Ingress Model Based on Turbulent Transport," ASME Turbo Expo 2017, Paper No. GT2017-63531, Charlotte, NC.
[4] Owen, J.M., 2012, "Theoretical modelling of hot gas ingestion through turbine rim seals," *Propulsion and Power Research*, **1**(1), pp. 1-11.
[5] Gentilhomme, O.J.P., 2004, "Turbine rim seal ingestion," PhD Dissertation, University of Sussex, Brighton, UK.
[6] Graber, D.J., Daniels, W.A., and Johnson, B.V., 1987, "Disc Pumping Test, Final Report," Air Force Wright Aeronautical Laboratories, Wright-Patterson AFB, Dayton, OH, Report No. AFWAL-TR-87-2050.
[7] Phadke, U.P. and Owen, J.M., 1988, "Aerodynamic aspects of the sealing of gas-turbine rotor-stator systems, Part 2: The performance of simple seals in a quasi-axisymmetric external flow," *Int. J. Heat and Fluid Flow*, **9**(2), pp. 106-112.
[8] Green, T. and Turner, A.B., 1992, "Ingestion into the Upstream Wheelspace of an Axial Turbine Stage," International Gas Turbine and Aeroengine Congress and Exposition, Paper No. 92-GT-303, Cologne, Germany.
[9] Owen, J.M., Wu, K., Scobie, J.A., Sangan, C.M., Cho, G., and Lock, G.D., 2015, "Use of Pressure Measurements to Determine Effectiveness of Turbine Rim Seals," *ASME J. Eng. Gas Turb. Power*, **137**(3), p. 032510.
[10] Bayley, F., J. and Owen, J. M., 1970, "The Fluid Dynamics of a Shrouded Disk System with a Radial Outflow of Coolant," *J. Eng. Power*, **92**(3), pp. 335–341.
[11] Phadke, U.P. and Owen, J.M., 1988, "Aerodynamic aspects of the sealing of gas-turbine rotor-stator systems, Part 3: The effect of nonaxisymmetric external flow on seal performance," *Int. J. Heat and Fluid Flow*, **9**(2), pp. 113-117.
[12] Popović, I. and Hodson, H.P., 2012, "The effects of a parametric variation of the rim seal geometry on the interaction between hub leakage and mainstream flows in HP turbines," ASME Turbo Expo 2012, Paper No. GT2012-68025, Copenhagen, Denmark.
[13] Kypuros, J.A. and Melcher, K.J., 2003, "A Reduced Model for Prediction of Thermal and Rotational Effects on Turbine Tip Clearance," National Aeronautics and Space Administration, Report No. NASA/TM—2003-212226.
[14] Nielsen, A.E., Moll, C.W., and Staudacher, S., 2005 "Modeling and Validation of the Thermal Effects on Gas Turbine Transients," *ASME J. Eng. Gas Turb. Power*, **127**(6), pp. 564-572.
[15] Amirante, D., Hills, N.J., and Barnes, C.J., 2012, "Use of dynamic meshes for transient metal temperature prediction," ASME Turbo Expo 2012, Paper No. GT2012-68782, Copenhagen, Denmark.
[16] Barringer, M., Coward, A., Clark, K., Thole, K., Schmitz, J., Wagner, J., Alvin, M. A., Burke P., and Dennis, R., 2014, "Development of a Steady Thermal Aero Research Turbine (START) for Studying Secondary Flow Leakages and Airfoil Heat Transfer," ASME Turbo Expo 2014, Paper No. GT2014-25570, Dusseldorf, Germany.
[17] Berdanier, R.A., Monge-Concepción, I., Knisely, B.F., Barringer, M.D., Thole, K.A., and Grover, E.A., 2019, "Scaling Sealing Effectiveness in a Stator-Rotor Cavity for Differing Blade Spans," *ASME J. Turbomach.*, **141**(5), p. 051007.
[18] Clark, K., Barringer, M., Johnson, D., Thole, K., Grover, E. and Robak, C., 2017, "Effects of Purge Flow Configuration on Sealing Effectiveness in a Rotor-Stator Cavity," *ASME J. Eng. Gas Turb. Power*, **140**(11), p. 112502.
[19] Berdanier, R.A. and Key, N.L., 2015, "Experimental Investigation of Factors Influencing Operating Rotor Tip Clearance in Multistage Compressors," *Int. J. Rotating Machinery*, **2015**, p. 146272.
[20] Figliola, R.S. and Beasley, D.E., 2011, *Theory and Design for Mechanical Measurements*, John Wiley & Sons, NY.
[21] Harvey, P.D., ed., 1982, *Engineering Properties of Steel*, American Society for Metals, Metals Park, OH.
[22] Clark, K., Barringer, M., Thole, K., Clum, C., Hiester, P., Memory, C., and Robak, C., 2016, "Using a Tracer Gas to Quantify Sealing Effectiveness for Engine Realistic Rim Seals," ASME Turbo Expo 2016, Paper No. GT2016-58095, Seoul, South Korea.